

# Single-layer group IV-V and group V-IV-III-VI semiconductors: Structural stability, electronic structures, optical properties, and photocatalysis

Jia-He Lin,<sup>1</sup> Hong Zhang,<sup>1,2,\*</sup> Xin-Lu Cheng,<sup>2</sup> and Yoshiyuki Miyamoto<sup>3</sup>

<sup>1</sup>College of Physical Science and Technology, Sichuan University, Chengdu 610065, China

<sup>2</sup>Key Laboratory of High Energy Density Physics and Technology of Ministry of Education, Sichuan University, Chengdu 610065, China

<sup>3</sup>Research Center for Computational Design of Advanced Functional Materials, National Institute of Advanced Industrial Science and Technology (AIST) Central 2, 1-1-1 Umezono, Tsukuba 305-8568, Japan

(Received 27 April 2017; revised manuscript received 30 June 2017; published 26 July 2017)

Recently, single-layer group III monochalcogenides have attracted both theoretical and experimental interest at their potential applications in photonic devices, electronic devices, and solar energy conversion. Excited by this, we theoretically design two kinds of highly stable single-layer group IV-V (IV = Si, Ge, and Sn; V = N and P) and group V-IV-III-VI (IV = Si, Ge, and Sn; V = N and P; III = Al, Ga, and In; VI = O and S) compounds with the same structures with single-layer group III monochalcogenides via first-principles simulations. By using accurate hybrid functional and quasiparticle methods, we show the single-layer group IV-V and group V-IV-III-VI are indirect bandgap semiconductors with their bandgaps and band edge positions conforming to the criteria of photocatalysts for water splitting. By applying a biaxial strain on single-layer group IV-V, single-layer group IV nitrides show a potential on mechanical sensors due to their bandgaps showing an almost linear response for strain. Furthermore, our calculations show that both single-layer group IV-V and group V-IV-III-VI have absorption from the visible light region to far-ultraviolet region, especially for single-layer SiN-AlO and SnN-InO, which have strong absorption in the visible light region, resulting in excellent potential for solar energy conversion and visible light photocatalytic water splitting. Our research provides valuable insight for finding more potential functional two-dimensional semiconductors applied in optoelectronics, solar energy conversion, and photocatalytic water splitting.

DOI: [10.1103/PhysRevB.96.035438](https://doi.org/10.1103/PhysRevB.96.035438)

## I. INTRODUCTION

Because of their unique atomic layer structures, two-dimensional (2D) materials have shown their extraordinary physical or chemical properties and great potential of application, which makes 2D materials become a rapid growing research direction in condensed matter physics. Graphene, a monolayer of carbon atoms arranged in a planar honeycomb lattice with Dirac cones at the Fermi level, exhibits impressive mechanical properties, high carrier mobility, wide band absorption, and other exotic behaviors [1–3]. However, the semimetallic electronic structure of graphene severely limits its functionality in semiconductor technology such as the applications on transistors and photocatalysts. This motivated research, both theoretical and experimental, on the search for novel 2D semiconducting materials beyond graphene. In recent decades, research on 2D materials, including single-layer group IV [4], single-layer group V [5–13], single-layer group III-V compound [14,15], and 2D transition-metal dichalcogenides [16–19], has made progress. Both single-layer MoS<sub>2</sub> and black phosphorene with a naturally occurring parent layered material have been successfully synthesized. The single-layer MoS<sub>2</sub> shows valley-dependent electronic properties and has a relatively sizable bandgap that reveals the viability of controlling the on and off currents in use as electron devices [17,20,21]. The black phosphorene has a direct bandgap and exhibits as remarkably anisotropic [22–24]. Furthermore, based on current technology conditions, even though some 2D

materials are only theoretically stable through computational analysis and without a naturally occurring parent layered material, it is also possible to experimentally synthesize them just like silicene, germanene, and stanene [25–27]. Therefore, the theoretical study has become a forerunner to discover more novel 2D materials.

Recently, systematic theoretical research has shown that monolayer group III monochalcogenides ( $MX$ ,  $M = \text{B, Ga, Al, and In}$ ;  $X = \text{O, S, Se, and Te}$ ) [28] are thermally stable semiconductors with indirect bandgaps which span a wide optical spectrum from deep ultraviolet (UV) to near infrared. Among these  $MX$  materials, single-layer GaS, GaSe, and GaTe have been experimentally synthesized, and the studies of their electronic and optical properties reveal that they have great potential applications in photonic devices and electronic devices [29–35]. In a theoretical study, single-layer  $MX$  ( $M = \text{Ga and In}$ ;  $X = \text{S, Se, and Te}$ ) is suggested as a potential photocatalyst for water splitting when the band edge position is compared with the redox potential of water [36]. Thus, single-layer  $MX$  is a functional material with great application potential. Just in time, a theoretical study has recently reported a  $P-6m2$  phase of single-layer silicon phosphide (SiP) material with high stability that consists of four sublayers stacked in the sequence P-Si-Si-P, which is the same with the structures of single-layer  $MX$ . This study also shows that the band structure of the  $P-6m2$  phase of single-layer SiP is very similar to single-layer GaTe [37]. According to these similarities between single-layer  $MX$  and SiP, it is reasonable to surmise that there is a stable class of single-layer group IV-V compounds like single-layer  $MX$ . If so, an interesting question is whether chemical and physical

\*hongzhang@scu.edu.cn

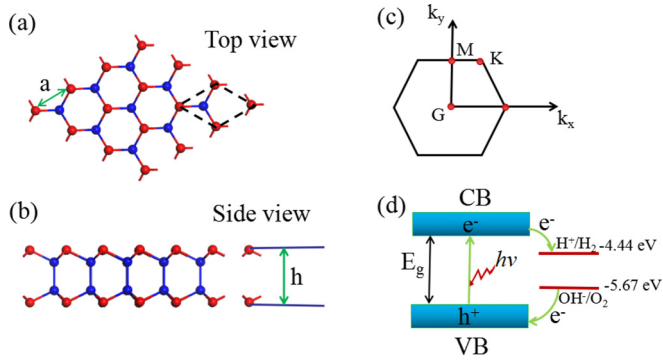


FIG. 1. (a) and (b) Top and side views of the single-layer group IV-V structure, respectively, marked with their structural parameters. The blue and red spheres stand for group IV and group V atoms, respectively. (c) Brillouin zone of the single-layer group IV-V and main high symmetric points. (d) Illustration of photocatalytic water splitting. The band edge positions of a photocatalysts must be aligned with reference to the redox potentials for water splitting.

properties, such as electronic structures, optical properties, and photocatalysis, of single-layer group IV-V compounds share similar features with single-layer  $MX$  or beyond. Furthermore, another question is whether a kind of single-layer of combined structures that consist of sublayers stacked in the sequence V-IV-III-VI can be stable and have more attractive properties than the single-layer  $MX$  and single-layer group IV-V compounds. The answers to the above questions are not only scientifically important to broaden our current knowledge of 2D materials, but also can provide a practical approach for the discovery of more novel 2D functional materials.

In this paper, we theoretically design a kind of 2D group IV-V compound ( $IV = \text{Si, Ge, and Sn}$ ;  $V = \text{N and P}$ ), which consists of four sublayers stacked in the sequence V-IV-IV-V, as shown in Figs. 1(a)–1(b). The space-group symmetry of the single-layer group IV-V is  $P-6m2$ , and their structures are similar to single-layer group III monochalcogenides. We carry out the phonon spectrum and cohesive energy of single-layer group IV-V compounds to prove that they are highly stable. The band structures of single-layer group IV-Vs are studied, which show that single-layer group IV-Vs are semiconductors. We show that these single-layer group IV-Vs meet the criteria of photocatalysts for water splitting [shown in Fig. 1(d)]. We also study how mechanical biaxial strains can be used to tune the bandgaps, band edge positions, and optical absorption of the single-layer group III to increase the potential efficiency of solar energy conversion and water splitting. Furthermore, in order to prove the possibility of our hypothesis about combined structures that consist of sublayers stacked in the sequence V-IV-III-VI, the single-layer group V-IV-III-VI compounds ( $IV = \text{Si, Ge, and Sn}$ ;  $V = \text{N and P}$ ;  $III = \text{Al, Ga, and In}$ ;  $VI = \text{O and S}$ ) are theoretically studied. Through the calculations of the phonon spectrum and cohesive energy, we find that single-layer group V-IV-III-VI compounds are highly stable. For comparing with the electronic properties, optical properties, and photocatalysis of single-layer group V-IV, the bandgaps, band edge positions, and absorption spectrum of single-layer group V-IV-III-VI are carried out.

This paper is organized as follows. In Sec. II, we describe the computational details employed in this paper. In Sec. III A, we analyze the stability of single-layer group IV-Vs ( $IV = \text{Si, Ge, and Sn}$ ;  $V = \text{N and P}$ ). In Sec. III B, we study the electronic structures of these six types of single-layer group IV-Vs. In Sec. III C, we identify that single-layer group IV-Vs are potential photocatalysts for water splitting. In Sec. III D, we study how biaxial strain impacts the bandgaps, band edge positions, and optical absorption of the single-layer group IV-Vs, and we obtain the ultimate biaxial tensile strain for these single-layer group IV-Vs to enhance the efficiency of solar energy conversion. In Sec. III E, we study electronic properties, optical properties, and photocatalysis of single-layer group V-IV-III-VIs ( $IV = \text{Si, Ge, and Sn}$ ;  $V = \text{N and P}$ ;  $III = \text{Al, Ga, and In}$ ;  $VI = \text{O and S}$ ). Finally, in Sec. IV, we summarize our results.

## II. COMPUTATIONAL DETAILS

All our calculations were obtained from first-principles density functional theory (DFT). The CASTEP [38] package was used with norm-conserving pseudopotentials and a plane-wave cutoff energy of 500 eV to relax the structure models and calculate the phonon dispersions and the band structures. For the structural relaxations and calculating the phonon dispersions, we employed the generalized gradient approximation (GGA) expressed by the Perdew-Burke-Ernzerhof (PBE) functional [39]. All of the structure models were fully relaxed, including the cells of single-layer group IV-V and group V-IV-III-VI, until the forces were smaller than 0.01 eV/Å and the energy tolerances were less than  $5 \times 10^{-6}$  eV per atom. A vacuum of 25 Å between these 2D single-layer structures was used. We adopt the Monkhorst-Pack scheme for k-point sampling of the Brillouin zone with  $20 \times 20 \times 1$  for single-layer group IV-V and group V-IV-III-VI. The phonon dispersions of single-layer group IV-V and group V-IV-III-VI were calculated by the linear response method [40]. Primitive cells were used for single-layer group IV-V and group V-IV-III-VI. The band structures were evaluated by the screened hybrid functional of Heyd-Scuseria-Ernzerhof (HSE06) [41].

To further study the stability of these materials, we performed finite temperature molecular dynamics simulations at 300 K for room temperature with  $6 \times 6 \times 1$  supercells containing 144 atoms by using the Vienna *Ab initio* Simulation Package (VASP). The length of time-step is chosen as 5 fs, and simulations with 1000 steps are executed. Due to the large number of atoms and the limit of computing resource, we used the  $1 \times 1 \times 1$  k-mesh and energy tolerances less than  $1 \times 10^{-4}$  eV per atom. Considering that the excitonic effects due to reduced screening in 2D systems influence the optical properties of single-layer group IV-V and group V-IV-III-VI, the many-body interactions (i.e., electron-electron and electron-hole interaction) must be taken into account for a correct description of the optical properties [42–45]. In this paper, we study the optical absorption spectrum and excitonic effects by using Green's function  $G$  and the screened Coulomb interaction  $W$  (GW) + the Bethe-Salpeter equation (BSE) as implemented in the VASP [46–49]. The GW + BSE calculations are performed on an  $8 \times 8 \times 1$  k-mesh within the Monkhorst-Pack scheme. The calculations were done in the following steps. Firstly,

DFT calculations are performed by using PBE-derived wave functions with an energy tolerance less than  $1 \times 10^{-8}$  eV per atom and a 500 eV energy cutoff for the wave functions. Secondly, based on the first step, we restart DFT calculations, which use exact diagonalization of the Hamiltonian and add 160 empty bands. Thirdly, based on the second step, one-shot GW (i.e.,  $G_0W_0$ ) calculations [50–55] are performed to obtain the quasiparticle excitations with a 200 eV energy cutoff for the response functions, and we use the spectral method and set the number of frequency points for 64. Finally, we carry out BSE calculations on top of  $G_0W_0$  in order to obtain the optical adsorption spectrum by including excitonic effects using the Tamm-Dancoff approximation [56]. In this section (BSE calculations), the eight highest occupied valence bands (VBs) and eight lowest unoccupied conduction bands (CBs) are included as a basis for the excitonic states with the photon energy region from 0 to 10 eV, in addition, a complex shift of  $\eta = 0.1$  eV is employed to broaden the calculated absorption spectrum.

### III. RESULTS AND DISCUSSION

#### A. Stability of single-layer group IV-V (IV = Si, Ge, and Sn; V = N and P)

After the full structural relaxations, we obtain the structural parameters, including lattice constants, bond length, layer height, and bond angle, of single-layer group IV-V, as shown in Figs. 1(a)–1(b). The corresponding values are summarized in Table I. In order to study the stability of single-layer group IV-V, we have carried out cohesive-energy calculations as well as phonon-dispersion calculations for single-layer group IV-V. To calculate the cohesive energy  $E_{\text{coh}}$  of single-layer group IV-V, we use the standard expression

$$E_{\text{coh}} = \frac{E_{\text{tot}} - 2E_{\text{atom}}(\text{IV}) - 2E_{\text{atom}}(\text{V})}{4}, \quad (1)$$

where  $E_{\text{tot}}$  is the total energy of single-layer group IV-V, and  $E_{\text{atom}}$  is the energy of a free atom, group IV, and group V, in its ground state, which is calculated from each isolated atom in a cubic cell with a 10 Å lattice constant, so as to avoid interactions between neighboring atoms. The cohesive energies of group IV nitride [see Table I] are  $-7.523$  eV (SiN),  $-6.324$  eV (GeN), and  $-6.578$  eV (SnN), and the cohesive energies of group IV phosphide are  $-5.404$  eV (SiP),  $-4.839$  eV (GeP), and  $-4.889$  eV (SnP). Because of the stronger ability of binding electrons of nitrogen atom, the

TABLE I. The results for optimized geometries and cohesive energies of single-layer group IV-V (IV = Si, Ge, and Sn; V = N and P) obtained using DFT with the PBE exchange-correlation functional.

Structure	Cohesive energy (eV/atom)	Lattice constant (Å) $a$	Layer height (Å) $h$
SiN	-7.523	2.907	3.549
GeN	-6.324	3.094	3.870
SnN	-6.578	3.263	4.154
SiP	-5.404	3.550	4.408
GeP	-4.839	3.693	4.645
SnP	-4.889	3.880	5.041

cohesive energies of group IV nitrides are relatively higher than the cohesive energies of group IV phosphides, which means that group IV nitrides are more stable than group IV phosphides. In addition, the high enough cohesive energies of single-layer group IV-V can be as used as evidence to prove that single-layer group IV-V may be highly stable.

Phonon calculations with no soft modes can provide a criterion to judge that these single-layer group IV-V compounds are dynamically stable. Therefore, in order to further confirm that these six types of single-layer group IV-V compounds are highly stable, phonon-dispersion calculations have been performed. The results of phonon dispersion along the high symmetric points in the Brillouin zone, as shown in Fig. 1(c), for these six structures are given in the left of Fig. 2. We find that the phonon dispersion is completely positive, and the minimum of the acoustic branch is linear around the  $G$  point, which demonstrates that these single-layer group IV-V compounds are kinetically stable. There is a common feature that the ionicity of group IV becomes stronger with the atomic number of the group IV atom increasing, reflecting on the degree of longitudinal optic-transverse optical (LO-TO) splitting of the optical branch. Moreover, there is a criterion to distinguish the group IV nitrides from the group IV phosphides through phonon dispersion. Due to the stronger ability of binding electrons of nitrogen atom, the ionicity of the group IV atom of the group IV nitride is stronger than the group IV atom of the group IV phosphide, and this results in the degree of LO-TO splitting of the group IV nitride being stronger than that of the group IV phosphide. In addition, we also have performed finite temperature molecular dynamics simulations at 300 K for room temperature to further study the stability of single-layer GeN and GeP, which are chosen to be the representatives of single-layer group IV-V, as shown in the right of Fig. 2. We find that the free energy curves as a function of time-step for single-layer GeN and GeP fluctuate around the equilibrium positions, and their crystal structures corresponding to the last free energy maximum in the  $T = 300$  K case, which are shown in the inset of the right of Fig. 2, still show no significant structural differences as compared with their initial crystal structures. This means that these materials can be stable at room temperature. Therefore, our calculations mentioned above provide an authentic test for the stability of single-layer group IV-V.

#### B. Band structures of single-layer group IV-V (IV = Si, Ge, and Sn; V = N and P)

The band structures of single-layer group IV-V, calculated from the HSE06 hybrid functional, are shown in Fig. 3. The bandgaps of group IV nitrides are 2.725 (SiN), 2.556 (GeN), and 1.873 (SnN) eV, as shown in Figs. 3(a)–3(c), and the bandgaps of group IV phosphides are 2.165 (SiP), 2.066 (GeP), and 2.165 (SnP) eV, as shown in Figs. 3(d)–3(f). Based on these, we find that, except for SnN, all the single-layer group IV-V materials are wide-bandgap 2D semiconductors with their bandgaps larger than 2.0 eV, which means that most single-layer group IV-V materials can be applicable to high-power electronic devices, field emission devices, and optoelectronic devices working under blue or UV light. Furthermore, it is obtained that all the single-layer group

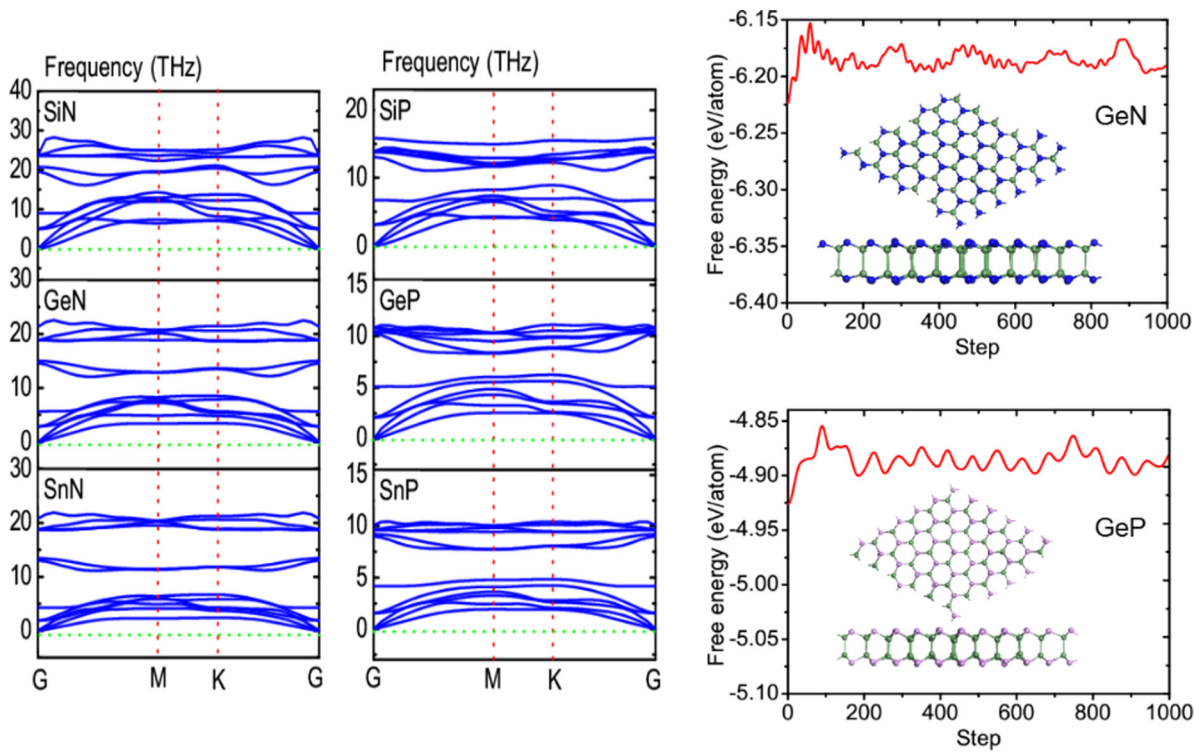


FIG. 2. Phonon band dispersions of single-layer group IV-V (IV = Si, Ge, and Sn; V = N and P) marked with their corresponding substance names, which exhibit outstanding kinetic stability, as shown on the left. For the finite temperature molecular dynamics simulations at 300 K, free energies as functions of time-step at temperature  $T = 300$  K and the crystal structures of single-layer GeN and GeP (see insets) corresponding to the last free energy maximum in the  $T = 300$  K case are shown on the right, which shows that single-layer GeN and GeP are stable at room temperature.

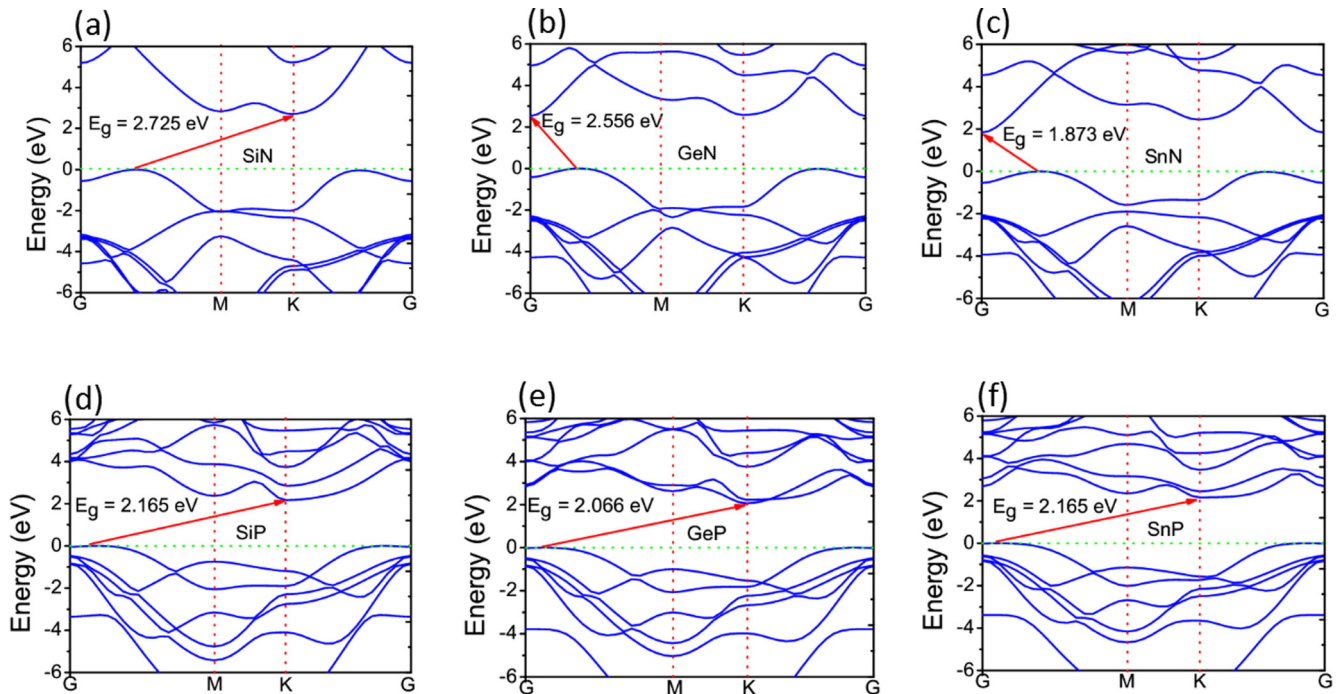


FIG. 3. (a)–(c) Band structures of single-layer SiN, GeN, and SnN, respectively. (d)–(f) Band structures of single-layer SiP, GeP, and SnP, respectively. The VBM is set to zero by green dash lines.

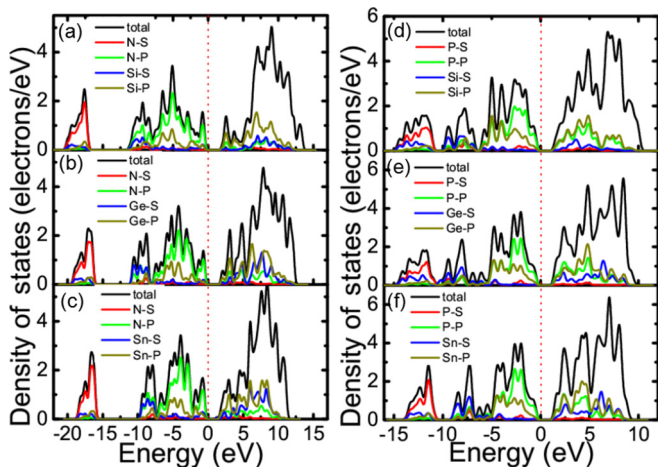


FIG. 4. (a)–(c) TDOS and PDOS of single-layer group IV nitrides (IV = Si, Ge, and Sn), respectively. (d)–(f) TDOS and PDOS of single-layer group IV phosphides (IV = Si, Ge, and Sn).

IV-V materials display indirect bandgaps. The VB maximum (VBM) of group IV nitride occurs along the  $G$ - $M$  direction, and the CB minimums (CBM) of both GeN and SnN lie at the  $G$  point, while the CBM of SiN lies at the  $K$  point. In addition, the VBM of group IV phosphide occurs along the  $G$ - $M$  direction, and the CBM of group IV phosphide lies at the  $K$  point.

In order to understand the contribution of different orbitals to the electronic states and the bonding characteristics of single-layer group IV-V, we carry out the calculations of the total densities of states (TDOS) and partial densities of states (PDOS) for single-layer group IV-V, and the results are shown in Fig. 4. As shown in Fig. 4, TDOS of all the single-layer group IV-V compounds exhibit multiple van Hove singularities over the entire energy range, which is consistent with the 2D nature of a single-layer material. It is observed from the PDOS of single-layer group IV-V that the states near the Fermi level have contributions from both the  $s$  and  $p$  orbitals of group IV and group V. The contributions from the  $p$  orbitals of group IV and group V to the TDOS are much higher than that from  $s$  orbitals. The fact that the  $p$  orbitals are dominant is caused by the  $sp^3$ -like bond of group IV and the  $sp^2$ -like bond of group V forming the single-layer group IV-V, and this feature always can be seen in diamondlike structures of group IV and monolayer honeycomb systems of group III. From the detailed analysis of PDOS, the states closest to the VBM of all the single-layer group IV-V materials have contributions from the  $p$  orbitals of group V. In case of the states closest to the CBM, the group IV nitride is different from the group IV phosphide. The states closest to the CBM of the group IV nitride have contributions from the  $p$  orbitals of group IV, while the states closest to the CBM of the group IV phosphide have contributions from the  $p$  orbitals of both group IV and group V. Additionally, the distribution of VBM and CBM in the single-layer group IV-V, especially for the group IV nitride, is beneficial for the separation of photogenerated electron-hole pairs, which is an important point for photocatalysis due to decreasing recombination of photogenerated electrons and holes to increase the photocatalytic activity [57].

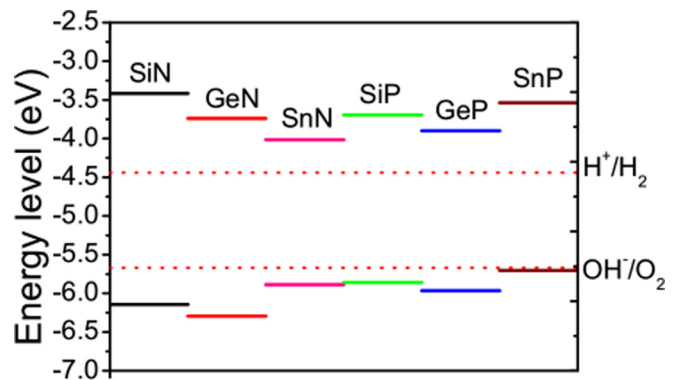


FIG. 5. Band edge positions of single-layer group IV-V (IV = Si, Ge, and Sn; V = N and P) relative to the vacuum level at zero strain calculated with the HSE06 functional. The standard redox potentials for water splitting are shown for comparison.

All of the bandgaps of single-layer group IV-V are in the visible light energy interval, which meets the bandgap requirement of photocatalysts for visible light splitting water. This indicates that the single-layer group IV-V materials could harvest a significant fraction of solar light and have a potential to be photocatalysts for visible light splitting water. Of course, to confirm whether these single-layer group IV-V materials are suitable for visible light splitting water, it is necessary to determine the alignment of the CBM and VBM energies with the redox potentials of water as well as a part of their absorption spectrum existing in the visible light region.

### C. Single-layer group IV-V (IV = Si, Ge, and Sn; V = N and P) for photocatalytic water splitting

We have calculated the work functions of single-layer group IV-V (IV = Si, Ge, and Sn; V = N and P) by using the HSE06 functional to determine the alignment of the CBM and VBM energies. Figure 5 compares the CBM and VBM energy levels with the redox potentials of water splitting. To become a promising candidate semiconductor for water splitting, it must be observed that both the reduction potential ( $V_{H^+/H_2} = 4.44$  eV) for  $H^+$  to  $H_2$  and the oxidation potential ( $V_{OH^-/O_2} = 5.67$  eV) for  $OH^-$  to  $O_2$  should be located inside the bandgap. As shown in Fig. 5, we find that the reduction level is obviously below the CBM of these single-layer group IV-V materials, which reveals that the reduction process is energetically favored. The oxidation level is obviously located in the bandgaps of the SiN, GeN, SnN, SiP, and GeP, while the VBM of SnP is slightly higher than the oxidation level, and this reveals that the oxidation on SnP is permitted presumably with a relatively low driving force. Therefore, these single-layer group IV-V materials can be deemed to be candidates as photocatalysts for water splitting. However, although our theoretical calculations predict that single-layer group IV-V meets the criteria of photocatalysts for water splitting in vacuum, the situation may change when it is kept in a liquid water environment. Therefore, further investigations are necessary to understand its band structure in a liquid water environment.

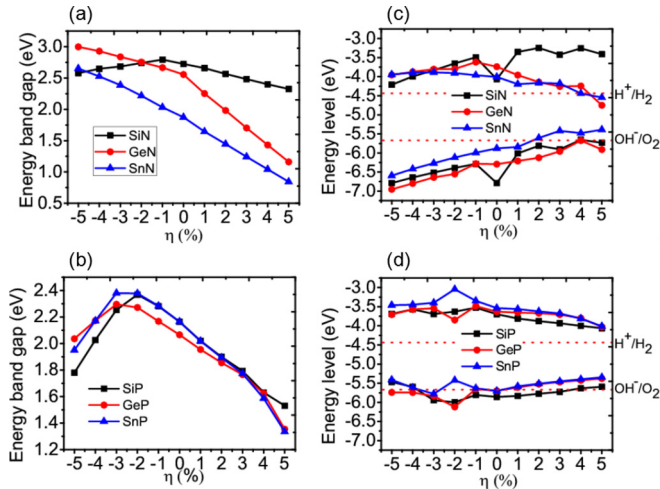


FIG. 6. (a) and (b) The changes of bandgaps for the group IV nitrides and group IV phosphides, respectively, with biaxial strain. (c) and (d) Strain effects on band edge positions of the group IV nitrides and group IV phosphides, respectively.

#### D. Tuning band structures and optical properties of single-layer group IV-V (IV = Si, Ge, and Sn; V = N and P) by biaxial strain

To be applied in real systems, strain effect is inevitable due to the synthetic environment and the application environment. Many experimental and theoretical [25,56,58–61] studies have shown that applying mechanical strain to the sample is a powerful method for modulating the band structures and the optical properties of materials. In the present case, we study the evolution of the band structures and the optical properties of single-layer group IV-V when it is subjected to mechanical biaxial strain, both tensile and compressive. The application of mechanical biaxial strain is simulated by freezing one of the lattice constants, which is different from the optimized value, and the biaxial strain can be represented by  $\eta = (a - a_0)/a_0$ , where  $a_0$  is the optimized lattice constant, and  $a$  is the lattice length along the strain direction. Positive and negative values of  $\eta$  stand for tensile and compressive, respectively. The bandgaps dependent on the strain  $\eta$  for the group IV nitride and the group IV phosphide are presented in Figs. 6(a) and 6(b), respectively, within a strain ranging from  $-5\%$  to  $5\%$  with a spacing of  $1\%$ . For the single-layer SiN [see black line in Fig. 6(a)], there are two linear variation tendencies of bandgaps. First, when  $\eta > -1\%$ , with the increase of  $\eta$ , the distance between Si atoms and N atoms is increasing, which makes the overlap integral of wave function between Si atoms and N atoms decrease and further leads to the

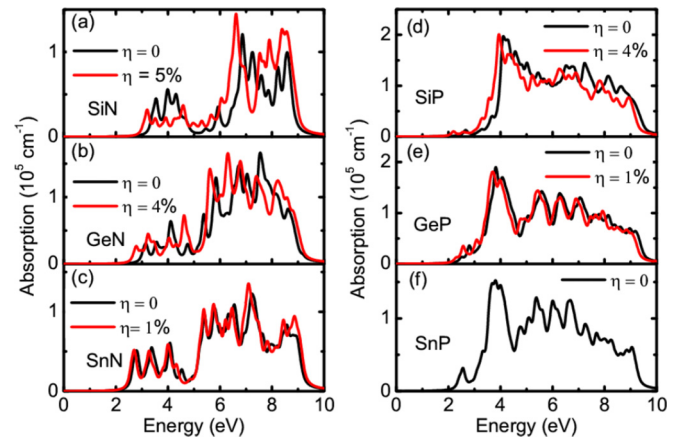


FIG. 7. (a)–(e) The absorption spectra of group IV-V except for single-layer SnP. (f) The absorption spectra of SnP. These absorption spectra are calculated by  $G_0W_0 + \text{BSE}$ . The black lines stand for their absorption spectra without strain, and the red lines stand for their absorption spectra with ultimate biaxial tensile strain as photocatalysts for water splitting.

decrease of its bandgaps. Second, when  $\eta \leq -1\%$ , with the decrease of  $\eta$ , the distance between neighboring Si atoms on the same sublayer becomes so close that the overlap integral of wave function for inner electrons of these Si atoms is increasing, which makes its bandgaps decrease. For the single-layer GeN [see red line in Fig. 6(a)], its bandgaps decrease with  $\eta$  increasing due to its layer height decreasing, and the variation tendency of bandgaps with  $\eta \leq -1\%$  is more gentle than the variation tendency of bandgaps with  $\eta > -1\%$ . For single-layer SnN [see blue line in Fig. 6(a)], mainly caused by its layer height decreasing, its bandgaps decrease with  $\eta$  increasing and represent an almost linear variation. It is clear that the bandgaps of the group IV nitride have a linear response with biaxial tensile strain, which means their potential to be a mechanical sensor. From Fig. 6(b), we see that all of the group IV phosphides have a common feature at the variation tendencies of bandgaps. When  $\eta \leq -2\%$  or  $-3\%$ , respectively, their bandgaps increase with  $\eta$  increasing, while their bandgaps decrease with  $\eta$  increasing with  $\eta > -2\%$  or  $-3\%$ , respectively.

To explore the effects of strain on the band edge positions of single-layer group IV-V, we have also carried out the corresponding CBM and VBM from the relaxed configurations through the calculations of work function, as can be seen in Figs. 6(c) and 6(d). Fig. 6(c), with biaxial compressive strain ( $-5\% \leq \eta < 0$ ), shows the group IV nitrides are still suitable

TABLE II. Quasiparticle bandgaps calculated by  $G_0W_0$ , optical gaps calculated by  $G_0W_0 + \text{BSE}$ , and the exciton binding energies of group IV-Vs without strain and with ultimate biaxial tensile strain as photocatalysts for water splitting. The quasiparticle bandgaps of SiP without strain accords with previous theoretical calculations by Huang *et al.* [37].

	SiN ( $\eta = 0$ )	SiN ( $\eta = 5\%$ )	GeN ( $\eta = 0$ )	GeN ( $\eta = 4\%$ )	SnN ( $\eta = 0$ )	SnN ( $\eta = 1\%$ )	SiP ( $\eta = 0$ )	SiP ( $\eta = 4\%$ )	GeP ( $\eta = 0$ )	GeP ( $\eta = 1\%$ )	SnP ( $\eta = 0$ )
$E_{G_0W_0}^{\text{gap}}$	3.62	3.12	3.16	2.71	2.38	2.26	2.63	2.38	2.44	2.33	2.66
$E_{\text{opt}}$	3.11	2.88	2.89	2.61	2.15	2.06	2.49	2.07	2.23	2.10	2.03
$E_{\text{bind}}$	0.51	0.24	0.27	0.10	0.23	0.20	0.14	0.31	0.21	0.23	0.63

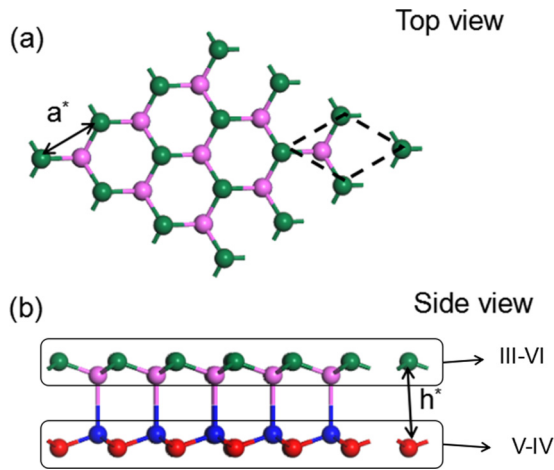


FIG. 8. (a) and (b) Top and side views of the group V-IV-III-VI (IV = Si, Ge, and Sn; V = N and P; III = Al, Ga, Ga, and In; VI = O and S), respectively. The blue, red, green, and pink spheres stand for group IV, group V, group III, and group VI atoms, respectively.

for photocatalytic water splitting. When it is biaxial tensile strain for group IV nitride, things are different. When  $\eta = 5\%$  for SiN,  $\eta = 4\%$  for GeN, and  $\eta = 1\%$  for SnN, the SiN, GeN, and SnN still meet the criteria of photocatalytic water splitting, and their bandgaps are 2.324, 1.430, and 1.645 eV, respectively. As shown in Fig. 6(d), when  $-3\% \leq \eta \leq 4\%$

SiP and  $-5\% \leq \eta \leq 1\%$  for GeP, the SiP and GeP are suitable photocatalysts for water splitting, while the SnP does not quite fit strain as a photocatalyst for water splitting so that strain effect should be lightened as far as possible during the synthesis and use. The bandgap of SiP is 1.631 eV at  $\eta = 4\%$ , and the bandgap of GeP is 1.955 eV at  $\eta = 1\%$ . Figure 6 provides useful guidance for tuning the bandgaps and CBM and VBM levels of single-layer group IV-V in order to maximize the efficiency of solar energy conversion. Then based on the data in Fig. 6, we will further calculate the absorption spectrum of single-layer group IV-Vs to investigate their utilization of sunlight.

We have carried out the absorption spectrum of single-layer group IV-V by the  $G_0W_0 + \text{BSE}$  method, which can take into full account many-body effects and excitonic effects. We focus on the absorption spectrum with in-plane polarization of light. We mainly study the absorption spectrum of these single-layer group IV-Vs without strain and with ultimate biaxial tensile strain for photocatalytic water splitting, except for single-layer SnP. To calculate the absorption spectrum, first, we calculate the frequency-dependent dielectric function  $\varepsilon(\omega) = \varepsilon_1(\omega) + i\varepsilon_2(\omega)$ , and then the absorption coefficient as a function of photon energy is evaluated according to the following expression [62]:

$$\alpha(E) = \frac{4\pi e}{hc} \left\{ \frac{[\varepsilon_1^2 + \varepsilon_2^2]^{1/2} - \varepsilon_1}{2} \right\}^{1/2}. \quad (2)$$

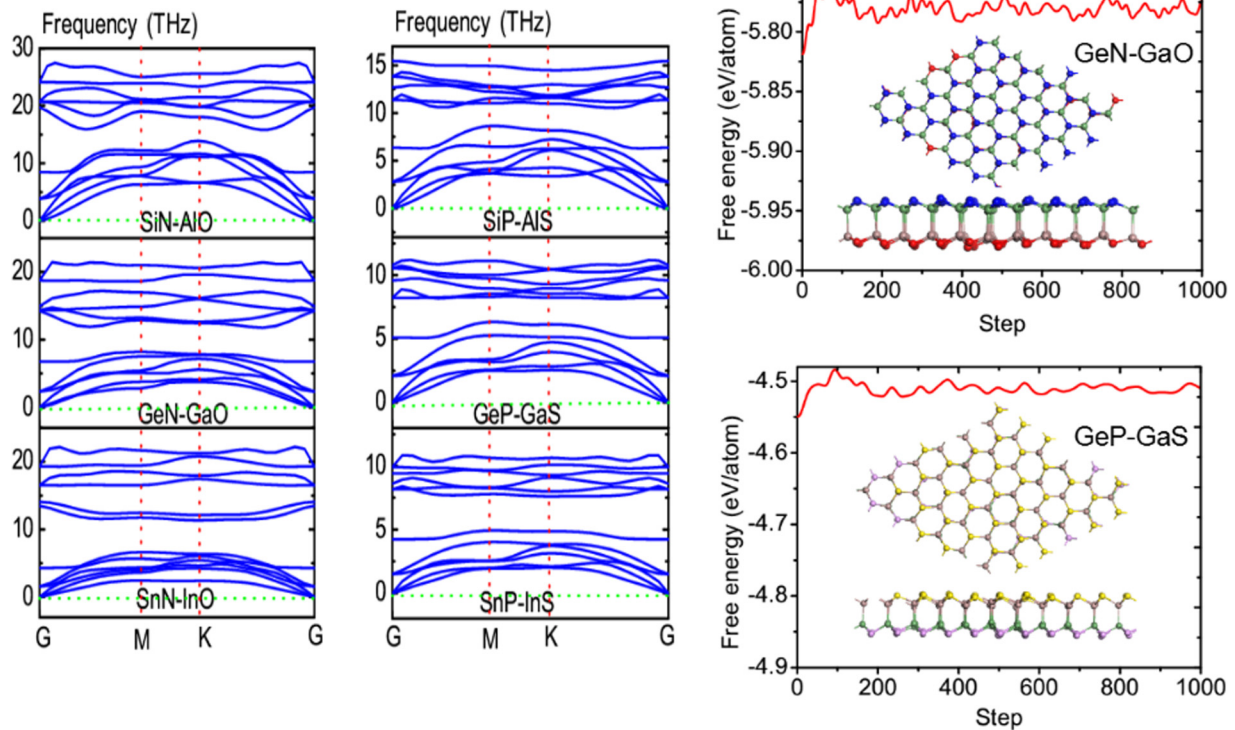


FIG. 9. Phonon band dispersions of single-layer group V-IV-III-VI (IV = Si, Ge, and Sn; V = N and P; III = Al, Ga, and In; VI = O and S) marked with their corresponding substance names, which exhibit outstanding kinetic stability, as shown in the left. For the finite temperature molecular dynamics simulations at 300 K, free energies as functions of time-step at temperature  $T = 300$  K and the crystal structures of single-layer GeN-GaO and GeP-GaS (see insets) corresponding to the last free energy maximum in the  $T = 300$  K case are shown on the right, which shows that single-layer GeN-GaO and GeP-GaS are stable at room temperature.

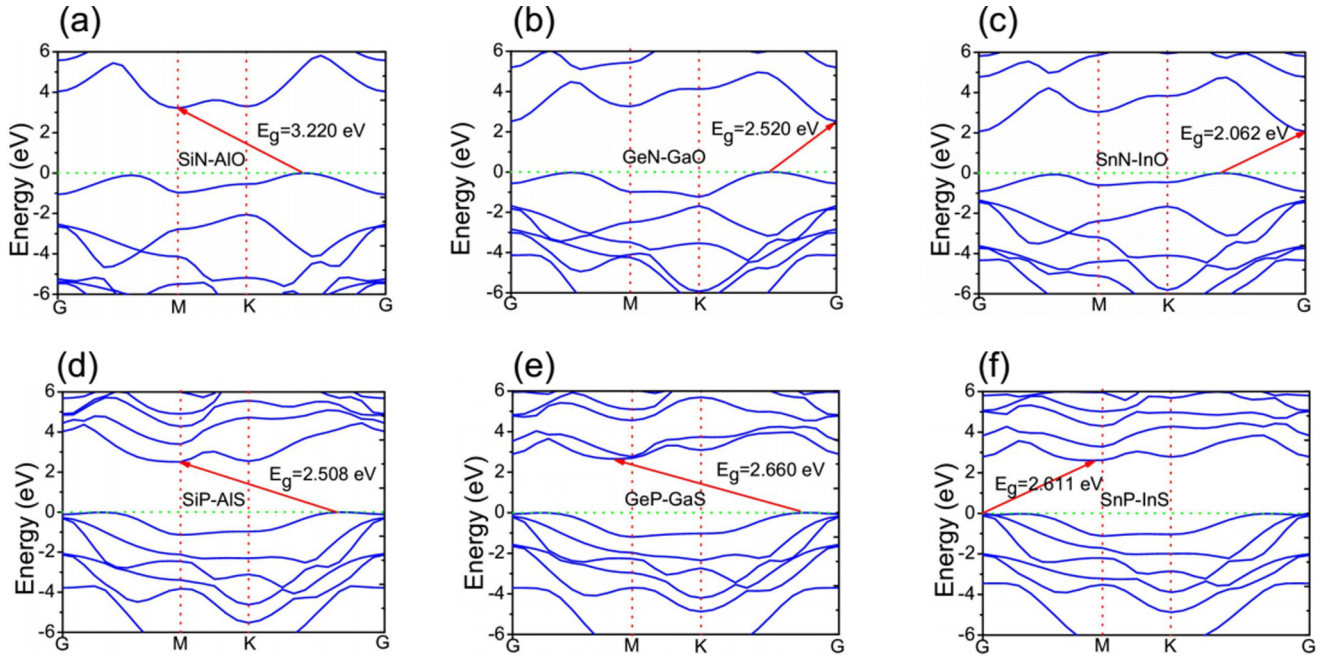


FIG. 10. Band structures of single-layer group V-IV-III-VI calculated with the HSE06 functional. (a)–(c) Band structures of single-layer SiN-AIO, GeN-GaO, and SnN-InO, respectively. (d)–(f) Band structures of single-layer SiP-AIS, GeP-GaS, and SnP-InS, respectively. The VBM is set to zero by green dash lines.

The results are shown in Fig. 7. Through the optical gaps ( $E_{\text{opt}}$ ) and the quasiparticle bandgaps ( $E_{G_0W_0}^{\text{gap}}$ ), the exciton binding energies ( $E_{\text{bind}} = E_{G_0W_0}^{\text{gap}} - E_{\text{opt}}$ ) are calculated, and the results are listed in Table II, which reveals that the exciton binding energies can be tuned by strain, which means that suitable modification through strain may make it relatively easy to form a luminescence center in single-layer group IV-V as photoelectric devices. Our calculations show that these single-layer group IV-V compounds are able to absorb the visible light at the range of 2.0 ~ 3.11 eV, which indicates that single-layer group IV-V compounds can be photocatalysts for visible light water splitting. For the group IV nitride, there are two absorption modes: one is located at the low-energy region and another one is located at the high-energy region, as shown in Figs. 7(a)–7(c). However, for the group IV phosphide, there is only one absorption mode, and its main absorption peak is at the near-UV region, as shown in Figs. 7(d)–7(f). Compared with the group IV phosphides, the group IV nitrides are more active in the range of visible light. Moreover, there is a common feature that, with the atomic number of group IV increasing, the absorption spectrum is red-shifted. Comparing the absorption spectrum with strain and the absorption spectrum with ultimate biaxial tensile strain, we find that, after tensile strain, a redshift occurs mainly caused by their bandgaps decreasing. This means that suitable tensile strain can increase the range of the optical absorption of the group IV-V in the visible light region.

#### E. Electronic properties, optical properties, and photocatalysis of single-layer group V-IV-III-VI (IV = Si, Ge, and Sn; V = N and P; III = Al, Ga, and In; VI = O and S)

We cut half of single-layer group V-IV and group III monochalcogenides, while their atomic numbers were closing

into each other, to form a new kind of single-layer materials, called single-layer group V-IV-III-VI (IV = Si, Ge, and Sn; V = N and P; III = Al, Ga, and In; VI = O and S), as shown in Fig. 8. To prove that single-layer group V-IV-III-VI compounds are stable, their phonon dispersion and cohesive energy are carried out. Compared with the corresponding energies that are obtained from  $[E_{\text{coh}}(\text{single-layer group V-IV}) + E_{\text{coh}}(\text{single-layer group III-VI})]/2$ , we find that the cohesive energies of single-layer group V-IV-III-VI is obviously larger than them, which means that single-layer group V-IV-III-VI may be stable, and it is possible to form these six types of single-layer group V-IV-III-VI compounds by cutting half of single-layer group V-IV and group III monochalcogenides. Furthermore, learning from the phonon dispersion of single-

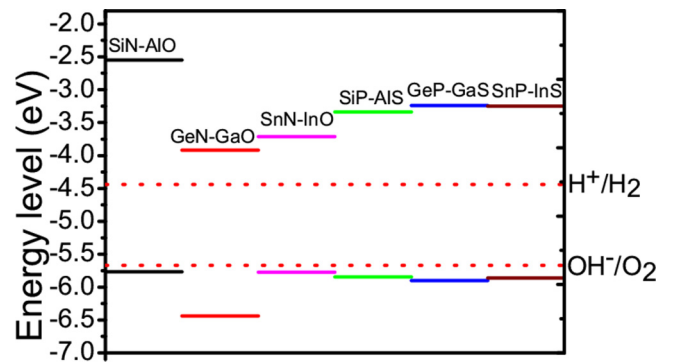


FIG. 11. Band edge positions of group V-IV-III-VI (IV = Si, Ge, and Sn; V = N and P; III = Al, Ga, and In; VI = O and S) relative to the vacuum level at zero strain calculated with the HSE06 functional. The standard redox potentials for water splitting are shown for comparison.

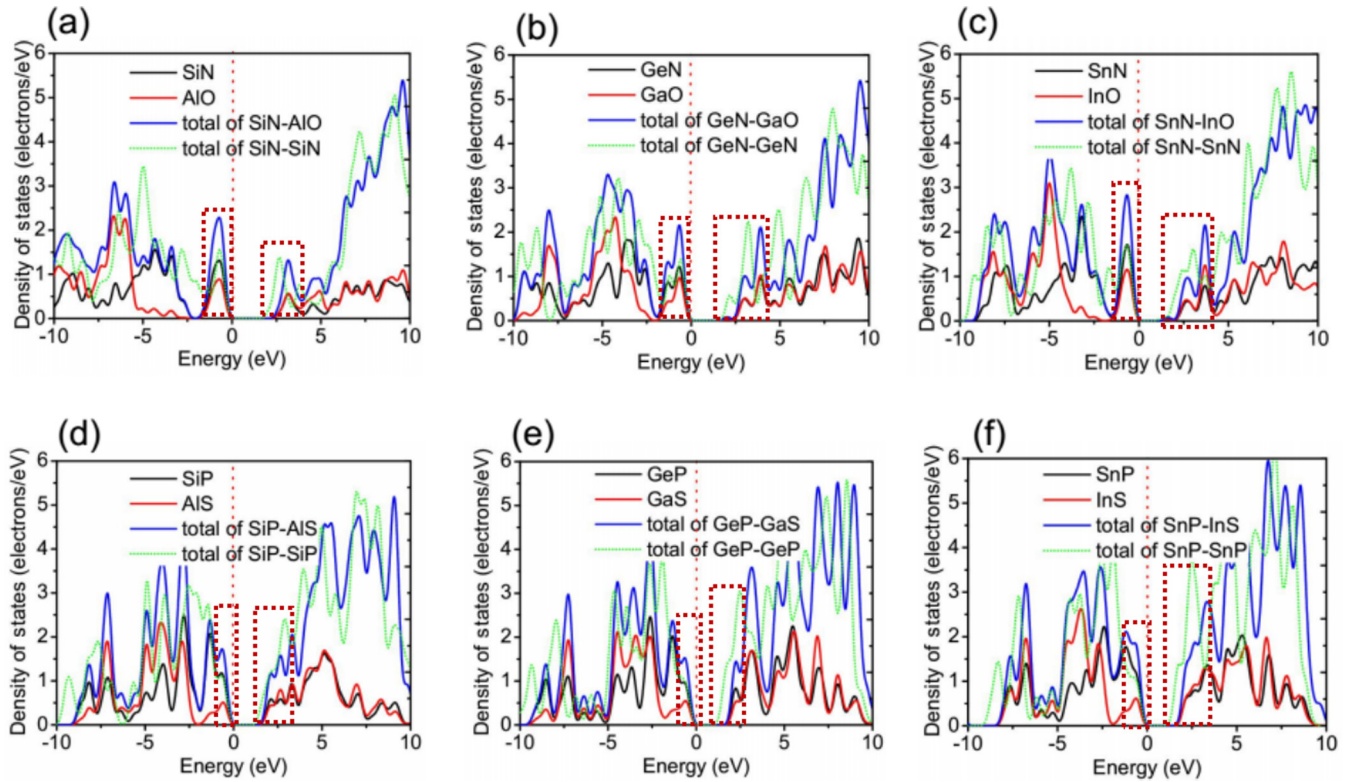


FIG. 12. (a)–(c) The densities of states (DOS) of single-layer SiN-AIO, GeN-GaO, and SnN-InO, respectively. (d)–(f) The DOS of single-layer SiP-AIS, GeP-GaS, and SnP-InS, respectively. The black and red lines are the PDOS of group V-IV and group III-VI of single-layer group V-IV-III-VI. The TDOS of single-layer group V-IV (green lines) are to compare with the DOS of single-layer group V-IV-III-VI. The red dotted line frames indicate the states that are near the CBM and VBM.

layer group V-IV-III-VI, we find that the phonon dispersion is completely positive and linear around the  $G$  point, which demonstrates that these six types of single-layer group V-IV-III-VI compounds are kinetically stable. We also have performed finite temperature molecular dynamics simulations at 300 K for room temperature to further study the stability of single-layer GeN-GaO and GeP-GaS, which were chosen to be the representatives of single-layer group V-IV-III-VI. The results show that single-layer GeN-GaO and GeP-GaS can be stable at room temperature, which means that single-layer group V-IV-III-VI can be stable at room temperature. The structure parameters and cohesive energy of single-layer group V-IV-III-VI as well as corresponding  $[E_{\text{coh}}(\text{single-layer group V-IV}) + E_{\text{coh}}(\text{single-layer group III-VI})]/2$  are shown in Table III. The phonon dispersion of single-layer group V-IV-III-VI and the finite temperature molecular dynamics simulations of single-layer GeN-GaO and GeP-GaS are shown in Fig. 9.

The band structures of single-layer group V-IV-III-VI calculated by HSE06 are different from the band structures of single-layer group V-IV, as shown in Fig. 10. As shown in Fig. 10, we find that all of single-layer group V-IV-III-VI compounds are indirect bandgap semiconductors, and their bandgaps are 3.220 eV (SiN-AIO), 2.520 eV (GeN-GaO), 2.062 eV (SnN-InO), 2.508 eV (SiP-AIS), 2.660 eV (GeP-GaS), and 2.611 eV (SnP-InS), respectively. Compared with corresponding group V-IV and group III monochalcogenides, the bandgaps of group V-IV-III-VI are larger. The VBM of group V-IV-III-VI occurs along the  $K$ - $G$  direction, while the VBM of single-layer SnP-InS lies at the  $G$  point. The CBM of single-layer SiN-AIO

and SiP-AIS lies at the  $M$  point. For single-layer GeN-GaO and SnN-InO, their CBMs lie at the  $G$  point. In the case of single-layer GeP-GaS and SnP-InS, their CBMs occur along the  $G$ - $M$  direction. We also have calculated the work functions of single-layer group V-IV-III-VI to determine the alignment of the CBM and VBM energies. Comparing the CBM and VBM energy levels with the redox potentials of water splitting shown in Fig. 11, we find that both the reduction potential and the oxidation potential are located inside the bandgaps

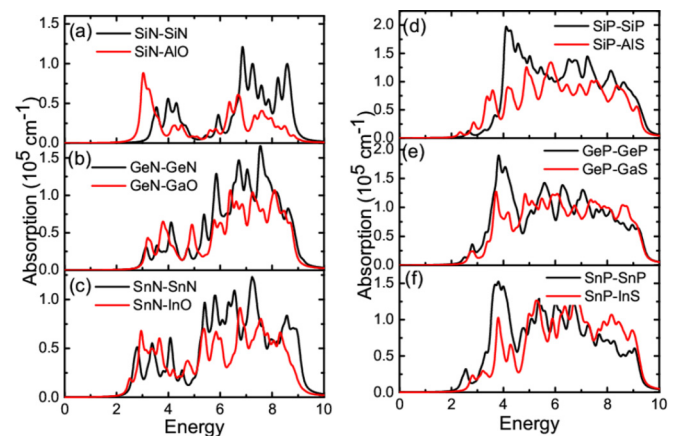


FIG. 13. The optical spectrum of single-layer group V-IV (black lines) and single-layer group V-IV-III-VI (red lines) calculated by  $G_0W_0 + \text{BSE}$ .

TABLE III. The results for optimized geometries and cohesive energies of single-layer group V-IV-III-VI (IV = Si, Ge, and Sn; V = N and P; III = Al, Ga, and In; VI = O and S) obtained using DFT with the PBE exchange-correlation functional.

Structure	Cohesive energy (eV/atom)	$[E_{\text{coh}}(\text{single-layer group V-IV}) + E_{\text{coh}}(\text{single-layer group III-VI})]/2$ (eV/atom)	Lattice constant (Å) $a^*$	Layer height (Å) $h^*$
SiN-AIO	-7.276	-6.626	2.882	3.693
GeN-GaO	-5.883	-5.422	3.101	3.943
SnN-InO	-6.570	-5.279	3.209	4.142
SiP-AIS	-5.152	-4.832	3.562	4.514
GeP-GaS	-4.501	-4.229	3.681	4.641
SnP-InS	-4.753	-4.104	3.832	4.974

of single-layer group V-IV-III-VI, which means that these single-layer group V-IV-III-VI compounds can be deemed to be candidates as photocatalysts for water splitting.

To make further investigation about the electronic properties of group V-IV-III-VI, we carry out their TDOS and PDOS. It is observed from Fig. 12 that the states near the Fermi level (approximately from -1.5 to 3.5 eV and marked by the red dotted line frames) have contributions from both groups V-IV and III-VI. For the states that are near the VBM, the contributions from group V-IV are obviously larger than the contributions from group III-VI. For the states that are near the CBM, the contributions from group V-IV are almost similar to the contributions from group III-VI. Interestingly, compared with the TDOS of group V-IV, the states that are near the VBM (approximately from -1.5 to 0 eV) contributed from group V-IV in group V-IV-III-VI are almost similar to that of group V-IV, and the TDOS of group V-IV-III-VI near the VBM are larger than that of group V-IV mainly caused by the contributions from group III-VI in group V-IV-III-VI. In addition, comparing the TDOS of group V-IV with the TDOS of group V-IV-III-VI near the CBM (approximately from 0 to 3.5 eV), the number of electrons for SiN-AIO, GeN-GaO, and SnN-InO are similar to that corresponding to group V-IV, as shown in Figs. 12(a)–12(c), while the number of electrons for SiP-AIS, GeP-GaS, and SnP-InS are much smaller than that corresponding to group V-IV, as shown in Figs. 12(d)–12(f). For single-layer SiN-AIO, GeN-GaO, and SnN-InO, these results may increase their transition probability of photon-generated electrons and improve their optical absorption in the low-energy region, but it may be quite the contrary to the case of single-layer SiP-AIS, GeP-GaS, and SnP-InS.

To further study the optical properties of single-layer group V-IV-III-VI, we have carried out their absorption spectrum by  $G_0W_0 + \text{BSE}$ , as shown in Fig. 13. It is obtained from Figs. 13(a)–13(c) that the optical absorption of single-layer SiN-AIO, GeN-GaO, and SnN-InO in the visible light region

becomes much stronger than that of single-layer SiN, GeN, and SnN. In the case of single-layer SiP-AIS, GeP-GaS, and SnP-InS, their optical absorption in the low-energy region is weaker than that of single-layer SiP, GeP, and SnP, which indicates that single-layer SiP, GeP, and SnP have greater potential in application on photoelectric devices, especially in the near-UV region than that of single-layer SiP-AIS, GeP-GaS, and SnP-InS. These results conform to our views obtained from the above analysis. Importantly, the first absorption peaks of single-layer SiN-AIO and SnN-InO that locate at 3 eV are strong, which means that both single-layer SiN-AIO and SnN-InO are excellent candidates for solar energy conversion and photocatalysts for visible light water splitting. We also have calculated the optical gaps and the quasiparticle bandgaps of single-layer group V-IV-III-VI to study their exciton binding energies, as shown in Table IV. We find that their exciton binding energies cover a range from 0.233 to 1.41 eV. For single-layer SiN-AIO and GeP-GaS, their exciton binding energies reach up to 1.41 and 1.03 eV, respectively, which means that they may be easy to form a luminescence center and have high luminous efficiency as photoelectric devices.

#### IV. CONCLUSIONS

In summary, we have theoretically studied single-layer group IV-V (IV = Si, Ge, and Sn; V = N and P) and group V-IV-III-VI (IV = Si, Ge, and Sn; V = N and P; III = Al, Ga, and In; VI = O and S) based on first-principles calculations. Through the calculations of the phonon spectrum, the finite temperature molecular dynamics simulations at 300 K, and cohesive energy, we predict that single-layer group IV-V and group V-IV-III-VI are highly stable. Our calculations of the bandgaps and band edge positions using accurate hybrid functional and quasiparticle methods indicate that both the single-layer group IV-V and group V-IV-III-VI are indirect bandgap semiconductors and suitable photocatalysts for water

TABLE IV. Quasiparticle bandgaps calculated by  $G_0W_0$ , optical gaps calculated by  $G_0W_0 + \text{BSE}$ , and the exciton binding energies of single-layer group V-IV-III-VI (IV = Si, Ge, and Sn; V = N and P; III = Al, Ga, and In; VI = O and S).

	SiN-AIO	GeN-GaO	SnN-InO	SiP-AIS	GeP-GaS	SnP-InS
$E_{G_0W_0}^{\text{gap}}$	3.93	3.38	2.53	3.16	3.59	3.10
$E_{\text{opt}}$	2.52	2.79	2.29	2.61	2.56	2.56
$E_{\text{bind}}$	1.41	0.59	0.24	0.55	1.03	0.54

splitting. By investigating the strain effect on single-layer group IV-V, we find that their bandgaps and band edge positions can be effectively adjusted by applying a biaxial strain. In addition, we find that the group IV nitrides perform more excellent than the group IV phosphides for being mechanical sensors due to group IV nitrides showing an almost linear response for strain. We also have studied the optical absorption of single-layer group IV-V without strain and with an ultimate biaxial tensile strain for photocatalytic water splitting. The results show that single-layer group IV-V compounds have absorption from the visible light region to the far-UV region, and an ultimate biaxial tensile strain can strengthen the optical absorption of single-layer group IV-V in the visible light region. Moreover, we have carried out the optical spectrum of single-layer group V-IV-III-VI. Our results shows that single-layer SiN-AIO and SnN-InO have strong

absorption in the visible light region, which means that these two types of single-layer group V-IV-III-VI compounds have excellent potential for solar energy conversion and visible light photocatalytic water splitting. All of our calculations provide valuable guidance for finding more 2D semiconductors for nanoelectronic, optoelectronic devices, and potential photocatalysts for water splitting.

#### ACKNOWLEDGMENTS

H.Z. and X.C. acknowledge financial support from the National Key R&D Program of China (2017YFA0303603) and National Natural Science Foundation of China (Grants No. 11474207 and No. 11374217). Y.M. acknowledges funding from JSPS KAKENHI with Grants No. JP16H00925 and No. JP16K05412.

- 
- [1] A. K. Geim and K. S. Novoselov, *Nat. Mater.* **6**, 183 (2007).  
 [2] F. Schwierz, *Nat. Nanotechnol.* **5**, 487 (2010).  
 [3] K. S. Novoselov, A. K. Geim, S. V. Morozov, D. Jiang, M. I. Katsnelson, I. V. Grigorieva, S. V. Dubonos, and A. A. Firsov, *Nature (London)* **438**, 197 (2005).  
 [4] C. C. Liu, H. Jiang, and Y. Yao, *Phys. Rev. B* **84**, 195430 (2011).  
 [5] L. Li, Y. Yu, G. J. Ye, Q. Ge, X. Ou, H. Wu, D. Feng, X. H. Chen, and Y. Zhang, *Nat. Nanotechnol.* **9**, 372 (2014).  
 [6] H. Liu, A. T. Neal, Z. Zhu, X. Xu, D. Tomanek, and P. D. Ye, *ACS Nano* **8**, 4033 (2014).  
 [7] A. Castellanos-Gomez, L. Vicarelli, E. Prada, J. O. Island, K. L. Narasimha-Acharya, S. I. Blanter, D. J. Groenendijk, M. Buscema, G. A. Steele, J. V. Alvarez, H. W. Zandbergen, J. J. Palacios, and H. S. J. van der Zant, *2D Mater.* **1**, 025001 (2014).  
 [8] F. Xia, H. Wang, and Y. Jia, *Nat. Commun.* **5**, 4458 (2014).  
 [9] S. P. Koenig, R. A. Doganov, H. Schmidt, A. H. Castro Neto, and B. Ozyilmaz, *Appl. Phys. Lett.* **104**, 103106 (2014).  
 [10] M. Buscema, D. J. Groenendijk, G. A. Steele, H. S. J. van der Zant, and A. Castellanos-Gomez, *Nat. Commun.* **5**, 4651 (2014); Q. Tang and Z. Zhou, *Prog. Mater. Sci.* **58**, 1244 (2013).  
 [11] Z. Zhu and D. Tomanek, *Phys. Rev. Lett.* **112**, 176802 (2014).  
 [12] S. Zhang, Z. Yan, Y. Li, Z. Chen, and H. Zeng, *Angew. Chem.* **127**, 3155 (2015).  
 [13] C. Kamal and M. Ezawa, *Phys. Rev. B* **91**, 085423 (2015).  
 [14] M. Wu, Z. Zhang, and X. Cheng Zeng, *Appl. Phys. Lett.* **97**, 093109 (2010).  
 [15] H. Şahin, S. Cahangirov, M. Topsakal, E. Bekaroglu, E. Akturk, R. T. Senger, and S. Ciraci, *Phys. Rev. B* **80**, 155453 (2009).  
 [16] B. Radisavljevic, A. Radenovic, J. Brivio, V. Giacometti, and A. Kis, *Nat. Nanotechnol.* **6**, 147 (2011).  
 [17] K. F. Mak, C. Lee, J. Hone, J. Shan, and T. F. Heinz, *Phys. Lett.* **105**, 136805 (2010).  
 [18] D. Braga, I. G. Lezama, H. Berger, and A. F. Morpurgo, *Nano Lett.* **12**, 5218 (2012).  
 [19] S. Tongay, W. Fan, J. Kang, J. Park, U. Koldemir, J. Suh, D. S. Narang, K. Liu, J. Ji, J. Li, R. Sinclair, and J. Wu, *Nano Lett.* **14**, 3185 (2014).  
 [20] Q. H. Wang, K. Kalantar-Zadeh, A. Kis, J. N. Coleman, and M. S. Strano, *Nat. Nanotechnol.* **7**, 699 (2012).  
 [21] X. Xu, W. Yao, D. Xiao, and T. F. Heinz, *Nat. Phys.* **10**, 343 (2014).  
 [22] X. F. Song and H. B. Zeng, *J. Mater. Chem. C* **1**, 2952 (2013).  
 [23] H. B. Zeng, C. Y. Zhi, Z. H. Zhang, X. L. Wei, X. B. Wang, W. L. Guo, Y. Bando, and D. Golberg, *Nano Lett.* **10**, 5049 (2010).  
 [24] Ting Cao, Gang Wang, Wenpeng Han, Huiqi Ye, Chuanrui Zhu, Junren Shi, Qian Niu, Pingheng Tan, Enge Wang, Baoli Liu, and Ji Fenga, *Nat. Commun.* **3**, 887 (2012).  
 [25] P. Vogt, P. De Padova, C. Quaresima, J. Avila, E. Frantzeskakis, M. C. Asensio, A. Resta, B. Ealet, and G. Le Lay, *Phys. Rev. Lett.* **108**, 155501 (2012).  
 [26] C. C. Liu, W. Feng, and Y. Yao, *Phys. Rev. Lett.* **107**, 076802 (2011).  
 [27] F. Zhu, W. Chen, Y. Xu, C. Gao, D. Guan, C. Liu, D. Qian, S.-C. Zhang, and J. Jia, *Nat. Mater.* **14**, 1020 (2015).  
 [28] S. Demirci, N. Avazli, E. Durgun, and S. Cahangirov, *Phys. Rev. B* **95**, 115409 (2017).  
 [29] S. X. Yang, Y. Li, X. Z. Wang, N. J. Huo, J.-B. Xia, S.-S. Li, and J. B. Li, *Nanoscale* **6**, 2582 (2014).  
 [30] A. Harvey, C. Backes, Z. Gholamvand, D. Hanlon, D. McAteer, H. C. Nerl, E. McGuire, A. Seral-Ascaso, Q. M. Ramasse, N. McEvoy, S. Winters, N. C. Berner, D. McCloskey, J. F. Donegan, G. S. Duesberg, V. Nicolosi, and J. N. Coleman, *Chem. Mater.* **27**, 3483 (2015).  
 [31] P. Hu, L. Wang, M. Yoon, J. Zhang, W. Feng, X. Wang, Z. Wen, J. C. Idrobo, Y. Miyamoto, D. B. Geohegan, and K. Xiao, *Nano Lett.* **13**, 1649 (2013).  
 [32] S. Lei, L. Ge, Z. Liu, S. Najmaei, G. Shi, G. You, J. Lou, R. Vajtai, and P. M. Ajayan, *Nano Lett.* **13**, 2777 (2013).  
 [33] W. J. Jie, X. Chen, D. Li, L. Xie, Y. Y. Hui, S. P. Lau, X. D. Cui, and J. H. Hao, *Angew. Chem., Int. Ed.* **54**, 1185 (2015).  
 [34] Z. X. Wang, K. Xu, Y. C. Li, X. Y. Zhan, M. Safdar, Q. Wang, F. M. Wang, and J. He, *ACS Nano* **8**, 4859 (2014).  
 [35] W. Huang, L. Gan, H. Li, Y. Ma, and T. Zhai, *Cryst. Eng. Commun.* **18**, 3968 (2016).  
 [36] H. L. Zhuang and R. G. Hennig, *Chem. Mater.* **25**, 3232 (2013).

- [37] B. Huang, H. L. Zhuang, M. Yoon, B. G. Sumpter, and S.-H. Wei, *Phys. Rev. B* **91**, 121401(R) (2015).
- [38] M. D. Segall, P. J. D. Lindan, M. J. Probert, C. J. Pickard, P. J. Hasnip, S. J. Clark, and M. C. Payne, *J. Phys.: Condens. Matter* **14**, 2717 (2002).
- [39] J. P. Perdew, K. Burke, and M. Ernzerhof, *Phys. Rev. Lett.* **77**, 3865 (1996).
- [40] S. Baroni, S. de Gironcoli, A. dal Corso, and P. Giannozzi, *Rev. Mod. Phys.* **73**, 515 (2001).
- [41] J. Heyd, G. E. Scuseria, and M. Ernzerhof, *J. Chem. Phys.* **124**, 219906 (2006).
- [42] D. Y. Qiu, F. H. da Jornada, and S. G. Louie, *Phys. Rev. Lett.* **111**, 216805 (2013).
- [43] H.-P. Komsa and A. V. Krasheninnikov, *Phys. Rev. B* **86**, 241201 (2012).
- [44] H.-P. Komsa and A. V. Krasheninnikov, *Phys. Rev. B* **88**, 085318 (2013).
- [45] A. Ramasubramaniam, *Phys. Rev. B* **86**, 115409 (2012).
- [46] G. Kresse and J. Furthmüller, *Comput. Mater. Sci.* **6**, 15 (1996).
- [47] G. Kresse and J. Furthmüller, *Phys. Rev. B* **54**, 11169 (1996).
- [48] E. E. Salpeter and H. A. Bethe, *Phys. Rev.* **84**, 1232 (1951).
- [49] G. Onida, L. Reining, and A. Rubio, *Rev. Mod. Phys.* **74**, 601 (2002).
- [50] L. Hedin, *Phys. Rev.* **139**, A796 (1965).
- [51] M. S. Hybertsen and S. G. Louie, *Phys. Rev. B* **34**, 5390 (1986).
- [52] R. W. Godby, M. Schlüter, and L. J. Sham, *Phys. Rev. B* **37**, 10159 (1988).
- [53] M. Shishkin and G. Kresse, *Phys. Rev. B* **74**, 035101 (2006).
- [54] M. Shishkin and G. Kresse, *Phys. Rev. B* **75**, 235102 (2007).
- [55] M. Shishkin, M. Marsman, and G. Kresse, *Phys. Rev. Lett.* **99**, 246403 (2007).
- [56] J. Paier, M. Marsman, and G. Kresse, *Phys. Rev. B* **78**, 121201 (2008).
- [57] X. Li, J. Zhao, and J. Yang, *Sci. Rep.* **3**, 1858 (2013).
- [58] B. Lalmi, H. Oughaddou, H. Enriquez, A. Kara, and S. Vizzini, *Appl. Phys. Lett.* **97**, 223109 (2010).
- [59] J. H. Wong, B. R. Wu, and M. F. Lin, *J. Phys. Chem. C* **116**, 8271 (2012).
- [60] R. J. Young, L. Gong, I. A. Kinloch, I. Riaz, R. Jalil, and K. S. Novoselov, *ACS Nano* **5**, 3079 (2011).
- [61] F. Liu, X. Y. Liu, and J. F. Kang, *Appl. Phys. Lett.* **98**, 213502 (2011).
- [62] J. Qiao, X. Kong, Z.-X. Hu, F. Yang, and W. Ji, *Nat. Commun.* **5**, 4475 (2014).